DOI: 10.1021/ic1009863

Inorganic Chemistry
Article

Theoretical Investigation on the Photophysical Properties of Model Ruthenium Complexes with Diazabutadiene Ligands $[Ru(bpy)_{3-x}(dab)_x]^{2+}$ ($x = 1-3$)

Thomas Guillon,[†] Martial Boggio-Pasqua,*[,†] Fabienne Alary,[†] Jean-Louis Heully,[†] Emilie Lebon,[‡] Pierre Sutra,[‡] and Alain Igau[‡]

[†]*Laboratoire de Chimie et Physique Quantiques, UMR 5626, IRSAMC, CNRS et Université de Toulouse, 118 route de Narbonne, 31062 Toulouse, France, and* [‡]*Laboratoire de Chimie de Coordination, UPR 8241, CNRS, 205 route de Narbonne, 31077 Toulouse, France*

Received May 18, 2010

In this study we report a theoretical comparative study of some photophysical properties in the $[Ru(bpy)_{3-x}(dab)_x]^{2+}$ ($x = 0-3$) series. Density functional theory calculations, validated by highly correlated ab initio benchmark calculations, were used to investigate the absorption and emission properties of the complexes with $x = 1-3$. The presence of a 1,4-diaza-1,3-butadiene (dab) ligand dramatically changes these properties because of the strong π-acceptor character of this ligand. As a result, comparing to the reference $[Ru(bpy)_3]^{2+}$ complex previously studied, we observed (i) a strong red-shift of the maximum of the absorption band, (ii) a strong decrease of the emission energy of the lowest triplet metal-to-ligand charge transfer state, with all the $[Ru(bpy)_{3-x}(dab)_x]^{2+}$ ($x = 1-3$) complexes luminescent in the near-infrared region, while $[Ru(bpy)_3]^{2+}$ emits in the visible region, and (iii) the triplet metal-centered states become inaccessible in all the $[Ru(bpy)_{3-x}(dab)_x]^{2+}$ ($x = 1-3$) complexes. Consequently, these complexes could be potential candidates for infrared light-emitting diodes and probes.

1. Introduction

Molecular architectures based on polypyridine complexes of d^6 metal ions such as Ru^{II} are currently among the most studied compounds in coordination chemistry. This is due to their unique photoreactivity, which stems partly from the nature of the triplet excited states whose redox properties are responsible for specific electron- and energy-transfer processes.[1,2] Numerous applications can be mentioned in the fields of photochemistry, photophysics, photocatalysis, and biochemistry.[1−7] For example, for potential applications in optoelectronics and luminescence-based technologies, polypyridine ruthenium complexes have been designed with long-lived room temperature photoluminescence.[8] Issues to be addressed in these studies include the determination of the energy position and properties of the excited states in mixed ligand (i.e., heteroleptic) systems, and the ability to tune these excited state properties with a judicious choice of ligands.[9]

The photophysical properties of the prototype $[Ru(bpy)_3]^{2+}$ (where bpy = 2,2′-bipyridine) and related complexes are now relatively well understood. The lowest energy transitions of these compounds are of the type metal-to-ligand charge transfer (MLCT). These complexes can, in principle, show an emission from their ^{3}MLCT states, but depopulation of these states toward triplet metal-centered (MC) states conditions their lifetime, luminescence quantum yield, and photostability. To design a long-lived photoluminescent candidate, one has to find a ruthenium complex with a ^{3}MLCT state sufficiently lower than the ^{3}MC state to improve the emission quantum yield. Most of the time, the choice of ligands is determined by models based on ligand field theory. Use of strong π-accepting ligands to stabilize the ^{3}MLCT state is one of the possible strategies. For instance, one can use a strong π-accepting polypyridine ligand, which is characterized by a low π^* manifold. Another strategy consists in destabilizing the ^{3}MC by strengthening the σ-donor properties of the ligand or by improving the octahedral character of the complex.[10] In our study, we have chosen the first approach: we have

*To whom correspondence should be addressed. E-mail: martial.boggio@irsamc.ups-tlse.fr.

(1) Juris, A.; Balzani, V.; Barigelletti, F.; Campagna, S.; Belser, P.; von Zelewsky, A. *Coord. Chem. Rev.* **1988**, *84*, 85–277.
(2) Campagna, S.; Puntoriero, F.; Nastasi, F.; Bergamini, G.; Balzani, V. *Top. Curr. Chem.* **2007**, *280*, 117−214, and references therein.
(3) Sun, L.; Hammarström, L.; Akermark, B. *Chem. Soc. Rev.* **2001**, *30*, 36–49.
(4) Burdinski, D.; Wieghardt, K.; Steenken, S. Q. *J. Am. Chem. Soc.* **1999**, *121*, 10781–10787.
(5) Gholamkhass, B.; Mametsuka, H.; Koike, K.; Tanabe, T.; Furue, M.; Ishitani, O. *Inorg. Chem.* **2005**, *44*, 2326–2336.
(6) Lachaud, F.; Quaranta, A.; Pellegrin, Y.; Dorlet, P.; Charlot, M.-F.; Un, S.; Leibl, W.; Aukauloo, A. *Angew. Chem., Int. Ed.* **2005**, *44*, 1536–1540.
(7) Barton, J. K. *Science* **1986**, *233*, 727–734.
(8) (a) Kozlov, D. V.; Tyson, D. S.; Goze, C.; Ziessel, R.; Castellano, F. N. *Inorg. Chem.* **2004**, *43*, 6083–6092. (b) Ji, S.; Wu, W.; Wu, W.; Song, P.; Han, K.; Wang, Z.; Liu, S.; Guo, H.; Zhao, J. *J. Mater. Chem.* **2010**, *20*, 1953–1963.
(9) Medlycott, E. A.; Hanan, G. S. *Chem. Soc. Rev.* **2005**, *34*, 133–142.
(10) Abrahamsson, M.; Jäger, M.; Kumar, R. J.; Österman, T.; Persson, P.; Becker, H.-C.; Johansson, O.; Hammarström, L. *J. Am. Chem. Soc.* **2008**, *130*, 15533–15542.

Published on Web 09/02/2010

Chart 1

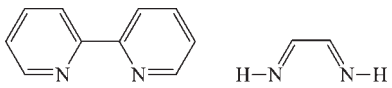

bpy dab

selected the simplest ligand among the diimine ligand family, the 1,4-diaza-1,3-butadiene (dab, Chart 1), because it has long been acknowledged that the dab ligand is a better π-acceptor than the bpy ligand.[11] Here we propose a predictive study of three ruthenium complexes, $[Ru(bpy)_{3-x}(dab)_x]^{2+}$ (with $x = 1-3$). As no X-ray and photophysical data are available yet for the $[Ru(bpy)_{3-x}(dab)_x]^{2+}$ ($x = 1-3$) series, the theoretical findings have been compared with those of the reference complex $[Ru(bpy)_3]^{2+}$, for which an identical theoretical procedure was used in references 12 and 13.

The aim of this work is to determine the main photophysical properties of the $[Ru(bpy)_{3-x}(dab)_x]^{2+}$ ($x = 1-3$) series. This includes the determination of the electronic absorption spectrum of each complex and to predict whether these new complexes could be good candidates as luminescent molecules. To work out such a prediction, we have determined the geometrical structures and energies of the low-lying triplet states (^{3}MLCT and ^{3}MC) as well as the topology of the triplet potential energy surface (PES) linking these structures, based on density functional theory (DFT) calculations.

DFT is a theoretical method commonly used to analyze the molecular and electronic structures of transition metal complexes. This method has been remarkably successful at evaluating a variety of ground state properties with high accuracy. The time-dependent generalization of DFT (TD-DFT) offers a rigorous way of calculating vertical electronic transitions (i.e., UV−visible spectra). Nevertheless, the reliability of the TD-DFT approach in obtaining accurate predictions of excitation energies in the case of long-range charge-transfer excited states is often called into question. Theoretically, this has been explained by Dreuw[14] and Hieringer,[15] who showed that in case of failure the whole TD-DFT calculation gives similar results to those obtained by taking the difference of the orbital energies of the lowest unoccupied molecular orbital (LUMO) and highest occupied molecular orbital (HOMO). In the work presented herein, we have checked that this was not the case, so there is no reason for concern in this case, and TD-DFT should be reliable for the low energy part of the spectrum we are investigating. Moreover, TD-DFT is known to describe the MLCT states of large ruthenium complexes correctly, by comparison of the computed absorption spectra with experimental ones[16,17] and in some cases with accurate multiconfigurational calculations (CASSCF/CASPT2).[18] As mentioned by Gorelsky et al.,[19] this is certainly due to the fact that MLCT states of those complexes are excited states of clear valence type. Also, in our case, the size of the ligands is not large, and the charge transfer involved is in a short-range.

Ab initio approaches are regarded today as the more accurate computational methods, but given the high computational cost involved, especially with large molecules, it is important to know how close the predictions between DFT and ab initio methods are. To check the reliability of our DFT approach, we performed for the first time highly correlated ab initio calculations on the $[Ru(dab)_3]^{2+}$ species, the modest size of this complex providing a great opportunity to compare the two types of approaches. The ab initio methods used are based on perturbation theory, coupled-cluster, and configuration interaction techniques.

The article is organized as follows: after some computational details, we present in section 3.1 the calculated optimized molecular structures and energy diagrams for the ground states of the $[Ru(bpy)_{3-x}(dab)_x]^{2+}$ ($x = 0-3$) complexes, followed in section 3.2 by their Franck−Condon excited states as given by TD-DFT. In this section, we also present the lowest triplet states for both MLCT and MC configurations and their emission energies calculated by Δ-SCF. In section 3.3, the topology of the triplet PES along the ^{3}MLCT→^{3}MC process is presented for each complex, and a discussion about the population of the ^{3}MC state is given. Finally, in section 3.4, the results of benchmark ab initio calculations are given to assess the reliability of the whole DFT approach.

2. Computational Details

DFT and TD-DFT calculations were performed using the Gaussian 03[20] and NWChem[21] packages. The B3LYP functional

(11) (a) Bock, H.; tom Dieck, H. *Angew. Chem.* **1966**, *78*, 549–550. *Angew. Chem., Int. Ed. Engl.* **1966**, *5*, 520−522. (b) Van Koten, G.; Vrieze, K. *Adv. Organomet. Chem.* **1982**, *21*, 151–239.
(12) Alary, F.; Heully, J.-L.; Bijeire, L.; Vicendo, P. *Inorg. Chem.* **2007**, *46*, 3154–3165.
(13) Alary, F.; Boggio-Pasqua, M.; Heully, J.-L.; Marsden, C. J.; Vicendo, P. *Inorg. Chem.* **2008**, *47*, 5259–5266.
(14) Dreuw, A.; Weisman, J. L.; Head-Gordon, M. *J. Chem. Phys.* **2003**, *119*, 2943–2946.
(15) Hieringer, W.; Görling, A. *Chem. Phys. Lett.* **2006**, *419*, 557–562.
(16) Bomben, P. G.; Robson, K. C. D.; Sedach, P. A.; Berlinguette, C. P. *Inorg. Chem.* **2009**, *48*, 9631–9643.
(17) Atsumi, M.; González, L.; Daniel, C. *J. Photochem. Photobiol. A: Chem.* **2007**, *190*, 310–320.
(18) (a) Turki, M.; Daniel, C.; Zális, S.; Vlcek, A., Jr.; van Slageren, J.; Stufkens, D. J. *J. Am. Chem. Soc.* **2001**, *123*, 11431–11440. (b) Zális, S.; Ben Amor, N.; Daniel, C. *Inorg. Chem.* **2004**, *43*, 7978–7985. (c) Ben Amor, N.; Zális, S.; Daniel, C. *Int. J. Quantum Chem.* **2006**, *106*, 2458–2469. (d) Vlcek, A.; Zális, S. *Coord. Chem. Rev.* **2007**, *251*, 258–287.
(19) Gorelsky, S. I.; Lever, A. B. P. *J. Organomet. Chem.* **2001**, *635*, 187–196.
(20) Frisch, M. J.; Trucks, G. W.; Schlegel, H. B.; Scuseria, G. E.; Robb, M. A.; Cheeseman, J. R.; Montgomery, Jr., J. A.; Vreven, T.; Kudin, K. N.; Burant, J. C.; Millam, J. M.; Iyengar, S. S.; Tomasi, J.; Barone, V.; Mennucci, B.; Cossi, M.; Scalmani, G.; Rega, N.; Petersson, G. A.; Nakatsuji, H.; Hada, M.; Ehara, M.; Toyota, K.; Fukuda, R.; Hasegawa, J.; Ishida, M.; Nakajima, T.; Honda, Y.; Kitao, O.; Nakai, H.; Klene, M.; Li, X.; Knox, J. E.; Hratchian, H. P.; Cross, J. B.; Bakken, V.; Adamo, C.; Jaramillo, J.; Gomperts, R.; Stratmann, R. E.; Yazyev, O.; Austin, A. J.; Cammi, R.; Pomelli, C.; Ochterski, J. W.; Ayala, P. Y.; Morokuma, K.; Voth, G. A.; Salvador, P.; Dannenberg, J. J.; Zakrzewski, V. G.; Dapprich, S.; Daniels, A. D.; Strain, M. C.; Farkas, O.; Malick, D. K.; Rabuck, A. D.; Raghavachari, K.; Foresman, J. B.; Ortiz, J. V.; Cui, Q.; Baboul, A. G.; Clifford, S.; Cioslowski, J.; Stefanov, B. B.; Liu, G.; Liashenko, A.; Piskorz, P.; Komaromi, I.; Martin, R. L.; Fox, D. J.; Keith, T.; Al-Laham, M. A.; Peng, C. Y.; Nanayakkara, A.; Challacombe, M.; Gill, P. M. W.; Johnson, B.; Chen, W.; Wong, M. W.; Gonzalez, C.; Pople, J. A. *Gaussian 03*, Revision D.01; Gaussian, Inc.: Wallingford, CT, 2004.
(21) Bylaska, E. J.; de Jong, W. A.; Kowalski, K.; Straatsma, T. P.; Valiev, M.; Wang, D.; Aprà, E.; Windus, T. L.; Hirata, S.; Hackler, M. T.; Zhao, Y.; Fan, P.-D.; Harrison, R. J.; Dupuis, M.; Smith, D. M. A.; Nieplocha, J.; Tipparaju, V.; Krishnan, M.; Auer, A. A.; Nooijen, M.; Brown, E.; Cisneros, G.; Fann, G. I.; Früchtl, H.; Garza, J.; Hirao, K.; Kendall, R.; Nichols, J. A.; Tsemekhman, K.; Wolinski, K.; Anchell, J.; Bernholdt, D.; Borowski, P.; Clark, T.; Clerc, D.; Dachsel, H.; Deegan, M.; Dyall, K.; Elwood, D.; Glendening, E.; Gutowski, M.; Hess, A.; Jaffe, J.; Johnson, B.; Ju, J.; Kobayashi, R.; Kutteh, R.; Lin, Z.; Littlefield, R.; Long, X.; Meng, B.; Nakajima, T.; Niu, S.; Pollack, L.; Rosing, M.; Sandrone, G.; Stave, M.; Taylor, H.; Thomas, G.; van Lenthe, J.; Wong, A.; Zhang, Z. *NWChem, A Computational Chemistry Package for Parallel Computers*, Version 5.0; Pacific Northwest National Laboratory: Richland, WA, 2006.

was used throughout with a fairly large basis set: a Stuttgart relativistic small-core effective potential[22] for ruthenium with its basis augmented by an f polarization function with an exponent of 0.96, a triple-ζ plus polarization basis set (Ahlrichs pVTZ)[23] was used for the C and N atoms, and a double-ζ plus polarization basis set (Ahlrichs pVDZ)[23] was used for H atoms. The DFT calculations were performed using the following strategy:

(i) DFT geometry optimizations were performed for the singlet ground state and triplet excited states of each complex, followed by analytical harmonic vibrational frequency calculations. Different symmetry constraints were used: D_3 symmetry for the homoleptic complex and C_2 symmetry for the heteroleptic complexes in their ground state; excited-state geometry optimizations were carried out in both D_3 and C_2 symmetry. In some cases, no symmetry constraint was imposed to verify that there were no lower energy structures that we could have missed. Geometry optimizations were performed with tight convergence criteria and an ultrafine integration grid. The stability of each unrestricted triplet wave function obtained was analyzed before computing the analytical harmonic vibrational frequencies. Atomic charges were derived by Weinhold's natural population analysis (NPA) using the natural orbital (NBO) partitioning scheme.[24]

(ii) TD-DFT calculations were performed at the ground-state geometry, which give the vertical absorption energies and the transition dipole moments. The first twenty roots for singlet states were computed, and the asymptotic correction of Hirata et al.[25] was included in the functional.

(iii) Δ-SCF calculations, which yield the energy difference between the triplet excited states at their optimized geometries and the closed-shell ground state at the same geometry, were performed. This is a simple and reliable way to obtain emission energies. All the triplet states were computed using unrestricted wave functions, whereas a restricted wave function was used for the singlet ground state. Spin contaminations of the unrestricted wave functions were found to be weak.

(iv) To determine the topology of the triplet PES along the ^{3}MLCT→^{3}MC reaction path, we performed linearly interpolated transit paths between the two excited-state structures obtained. Intermediate geometries were constructed by interpolating between the optimized geometries in internal coordinates.

Highly correlated ab initio methods were performed with Gaussian 03[20] and Molpro[26] packages. The energies of the ground state and of the lowest ^{3}MLCT and ^{3}MC excited states of the $[Ru(dab)_3]^{2+}$ were calculated at the corresponding optimized B3LYP structures. Ab initio geometry optimizations were carried out for the ground state. Among the highly correlated methods used are the complete active space second-order perturbation theory (CASPT2),[27] a recent method that couples the multireference configuration interaction technique with CASPT2 called CIPT2,[28] the Møller−Plesset perturbation theory from second order (MP2) up to fourth order (MP4),[29] the quadratic configuration interaction singles and doubles (QCISD),[30] and the coupled cluster singles and doubles (CCSD).[31] All these methods were used with the same basis sets as described above.

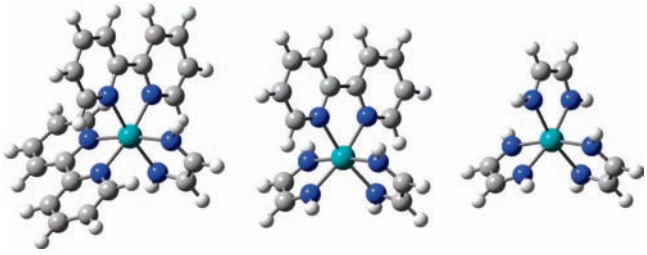

Figure 1. C_2 ground-state structures of $[Ru(bpy)_2(dab)]^{2+}$ and $[Ru(bpy)(dab)_2]^{2+}$, and D_3 ground-state structure of $[Ru(dab)_3]^{2+}$.

3. Results and Discussion

3.1. Ground State. 3.1.1. Molecular structures. Molecular structures of the three complexes are shown in Figure 1, and selected geometrical parameters of these complexes are reported in Table 1. NPA was carried out along with the evaluation of Wiberg bond indices (WBI) by performing NBO calculations at each ground state optimized structure. The results are collected in the last rows of Table 1.

In the computed structures of $[Ru(bpy)_{3-x}(dab)_x]^{2+}$ (x = 1−3) complexes, the environment of the ruthenium adopts, as usual, a distorted octahedral coordination geometry. The geometry of the ligands remains essentially unchanged within the three complexes. The main difference is the slightly shorter Ru−N bond with the dab ligand (2.04−2.06 Å) compared to the bpy ligand (2.10 Å), which is a consequence of the stronger metal−ligand binding for a strong π-acceptor ligand. The Ru−N bond lengths found are in good agreement with experimental crystal structures in which values ranging from 2.02 to 2.11 Å were found in substituted diazabutadiene Ru^0 complexes.[32−35]

The NBO analysis suggests that, as the number of dab ligands in the $[Ru(bpy)_{3-x}(dab)_x]^{2+}$ series increases, the metal becomes less electron rich, back-donation per ligand decreases, and the Ru−N bond lengths increase for both ligands. Here again, electronic density moves from ruthenium and bpy ligands toward the low π^* orbital of the dab ligand. The WBI values are consistent with a stronger interaction between Ru and the dab ligand compared

(22) Dolg, M.; Stoll, H.; Preuss, H.; Pitzer, R. M. *J. Phys. Chem.* **1993**, *97*, 5852–5859.
(23) Schäfer, A.; Horn, H.; Ahlrichs, R. *J. Chem. Phys.* **1992**, *97*, 2571–2577.
(24) Reed, A. E.; Curtiss, L. A.; Weinhold, F. *Chem. Rev.* **1988**, *88*, 899–926.
(25) Hirata, S.; Zhan, C.-G.; Aprà, E.; Windus, T. L.; Dixon, D. A. *J. Phys. Chem. A* **2003**, *107*, 10154–10158.
(26) Werner, H.-J.; Knowles, P. J.; Lindh, R.; Manby, F. R.; Schütz, M.; Celani, P.; Korona, T.; Rauhut, G.; Amos, R. D.; Bernhardsson, A.; Berning, A.; Cooper, D. L.; Deegan, M. J. O.; Dobbyn, A. J.; Eckert, F.; Hampel, C.; Hetzer, G.; Lloyd, A. W.; McNicholas, S. J.; Meyer, W.; Mura, M. E.; Nicklass, A.; Palmieri, P.; Pitzer, R.; Schumann, U.; Stoll, H.; Stone, A. J.; Tarroni, R.; Thorsteinsson, T. *MOLPRO*, version 2006.1, a package of ab initio programs; see http://www.molpro.net.
(27) Celani, P.; Werner, H.-J. *J. Chem. Phys.* **2000**, *112*, 5546–5557.
(28) Celani, P.; Stoll, H.; Werner, H.-J.; Knowles, P. J. *Mol. Phys.* **2004**, *102*, 2369–2379.
(29) Raghavachari, K.; Pople, J. A. *Int. J. Quantum Chem.* **1978**, *14*, 91–100.
(30) Pople, J. A.; Head-Gordon, M.; Raghavachari, K. *J. Chem. Phys.* **1987**, *87*, 5968–5975.
(31) Bartlett, R. J. *Annu. Rev. Phys. Chem.* **1981**, *32*, 359–401.
(32) Chaudret, B.; Cayret, C.; Köster, H.; Poilblanc, R. *J. Chem. Soc., Dalton Trans.* **1983**, 941–945.
(33) Rosenberger, V.; Fendesak, G.; tom Dieck, H. *J. Organomet. Chem.* **1991**, *411*, 445–456.
(34) Böttcher, L.; Scholz, A.; Walther, D.; Weisbach, N.; Görls, H. *Z. Anorg. Allg. Chem.* **2003**, *629*, 2103–2112.
(35) Xu, H.-J.; Lu, X.-Y.; Cheng, Y.; Sun, J.-F.; Chen, X.-T.; Xue, Z.-L. *Organometallics* **2009**, *28*, 6687–6694.

Table 1. Computational Results of the Main Bond Lengths (Å) and Bond Angles (deg) for the Ground State of $[Ru(bpy)_{3-x}(dab)_x]^{2+}$, $x = 0-3$[a]

	$[Ru(bpy)_3]^{2+}\ ^1A_1$	$[Ru(bpy)_2(dab)]^{2+}\ ^1A$	$[Ru(bpy)(dab)_2]^{2+}\ ^1A$	$[Ru(dab)_3]^{2+}\ ^1A_1$
		Geometry		
$Ru-N_{dab}$		2.040	2.046, 2.063	2.064
$Ru-N_{bpy}$	2.095	2.098, 2.107	2.099	
$(N-C)_{dab}$		1.300	1.295, 1.295	1.291
$(N-C)_{bpy}$	1.361	1.360, 1.360	1.360	
$(C-C)_{dab}$		1.442	1.448	1.454
$(C-C)_{bpy}$	1.472	1.472	1.472	
$(N-Ru-N)_{dab}$		75.9	75.4	75.3
$(N-Ru-N)_{bpy}$	78.0	77.6	77.8	
		NPA		
Ru	0.540	0.585	0.600	0.600
dab		0.330	2×0.400	3×0.470
bpy	3×0.490	2×0.542	0.603	
		WBI		
$Ru-N_{dab}$		0.576	0.540, 0.530	0.509
$Ru-N_{bpy}$	0.468	0.410, 0.430	0.425	

[a] Natural population analysis (NPA) and Wiberg bond indices (WBI) are also given.

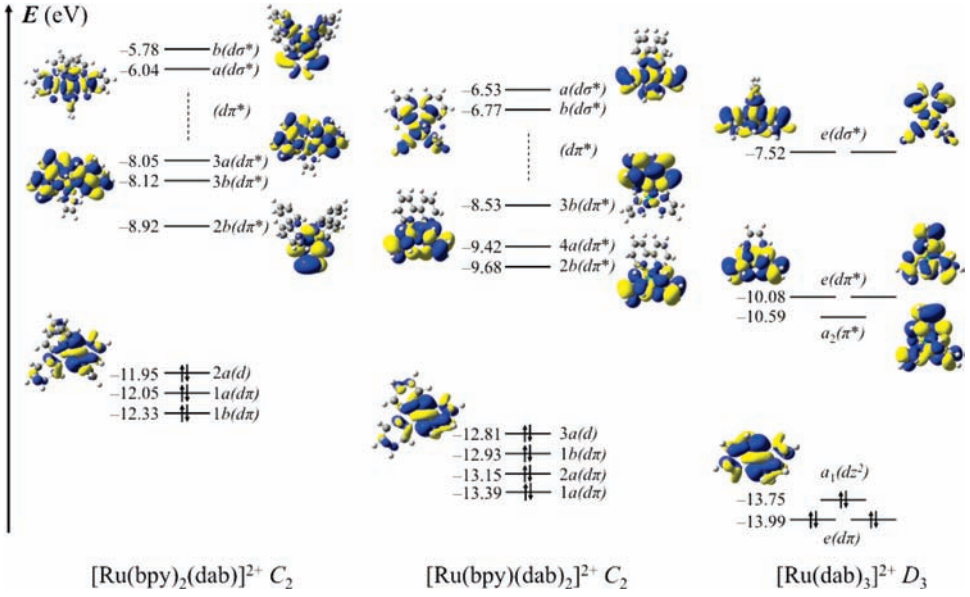

Figure 2. Simplified molecular orbital diagram of complexes in C_2 symmetry ($[Ru(bpy)_2(dab)]^{2+}$, $[Ru(bpy)(dab)_2]^{2+}$) and in D_3 symmetry ($[Ru(dab)_3]^{2+}$), where only the orbitals of interest are shown. The numbering of the orbitals was arbitrarily started at the lowest occupied orbital involved in the transitions shown in Table 2. Orbital eigenvalues are given in eV.

to the interaction between Ru and the bpy ligand. The consequence is a shorter Ru−N distance with the dab ligand relative to the Ru−N distance with the bpy ligand. Thus, a diminution of the coordination sphere is observed from $[Ru(bpy)_3]^{2+}$ to $[Ru(dab)_3]^{2+}$.

3.1.2. Energy Levels and Molecular Orbitals in the Ground State. Schematic d-block orbitals of the ground-state complexes are shown in Figure 2. In previous studies of homoleptic complexes, we have depicted in detail the d-block molecular orbitals.[12,13] The three highest occupied molecular orbitals of $[Ru(bpy)_{3-x}(dab)_x]^{2+}$ ($x = 1-3$) are mainly Ru(4d) orbitals, which correspond to the t_{2g} set in octahedral complexes. Their symmetries are $a_1(dz^2) + e$ in the D_3 point group, while they become $2a + b$ in the C_2 point group. The three lowest unoccupied orbitals are $a_2 + e$ and $a + 2b$ in the D_3 and C_2 point groups, respectively. The occupied molecular orbitals all decrease in energy, as the more σ-donor bpy is replaced by dab. In the homoleptic D_3 complex, there is no contribution from the d orbitals of the ruthenium atom in the LUMO, which belongs to the a_2 symmetry and is delocalized over the three ligands. For heteroleptic C_2 complexes, the Ru(4d) orbitals are more mixed with the dab π^* systems in the LUMO, as a consequence of the π-acceptor character of the dab ligands. As expected, the π^* orbitals of the dab ligands appear first in the virtual molecular orbital set; they are more stabilized than those of the bpy ligand. The HOMO−LUMO gaps of the complexes are calculated to be in the range 3.00−3.15 eV. Note that in previous calculations performed by Gorelsky and Lever[19] with a smaller basis set, the HOMO−LUMO gap slightly increases as x increases from 1 to 3.

Interestingly, when one reports the HOMO and LUMO energies in the $[Ru(bpy)_{3-x}(dab)_x]^{2+}$ ($x = 0-3$) series as a

Table 2. Selected TD-DFT Singlet Transition Energies (eV) for $[Ru(bpy)_2(dab)]^{2+}$, $[Ru(bpy)(dab)_2]^{2+}$, and $[Ru(dab)_3]^{2+}$ in Comparison with $[Ru(bpy)_3]^{2+}$

complex	transition[a]	nature of excitation[b]	composition of excitation
$[Ru(bpy)_3]^{2+}$	2.89,[c] *429* nm	MBCT	$e(d\pi)\rightarrow e(d\pi^*)$ $e(dz^2)\rightarrow e(d\pi^*)$
$[Ru(bpy)_2(dab)]^{2+}$	2.97 (0.090), *417* nm	MDCT	$1b(d\pi)\rightarrow 2b(d\pi^*)$ $2a(dz^2)\rightarrow 3a(d\pi^*)$
	3.10 (0.074), *400* nm	MBCT	$1a(d\pi)\rightarrow 3b(d\pi^*)$
$[Ru(bpy)(dab)_2]^{2+}$	2.90 (0.117), *428* nm	MDCT	$2a(d\pi)\rightarrow 2b(d\pi^*)$ $1b(d\pi)\rightarrow 4a(d\pi^*)$
	3.28 (0.077), *378* nm	MDCT	$1a(d\pi)\rightarrow 4a(d\pi^*)$ $2a(d\pi)\rightarrow 4a(d\pi^*)$
	4.27 (0.130), *290* nm	MBCT	$1a(d\pi)\rightarrow 3b(d\pi^*)$ $3a(dz^2)\rightarrow 4b(d\pi^*)$
$[Ru(dab)_3]^{2+}$	3.11 (0.310), *399* nm	MDCT	$e(d\pi)\rightarrow e(d\pi^*)$ $e(dz^2)\rightarrow e(d\pi^*)$

[a] Only transitions with oscillator strengths $f > 0.07$ are indicated. Values of f are in parentheses. Corresponding wavelengths are in italics. [b] MDCT: Metal-to-ligand charge transfer from Ru to the diazabutadiene(s). MBCT: Metal-to-ligand charge transfer from Ru to the bipyridine(s). [c] Experimental value of 2.74 eV.

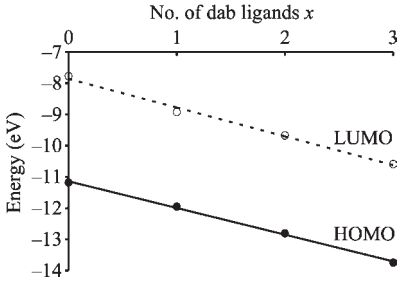

Figure 3. HOMO and LUMO energies reported as a function of the number of dab ligands in the $[Ru(bpy)_{3-x}(dab)_x]^{2+}$ ($x = 0-3$) series.

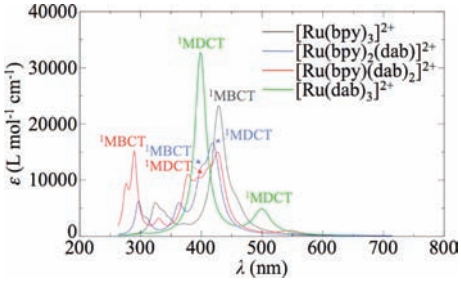

Figure 4. Simulated absorption spectra for $[Ru(bpy)_2(dab)]^{2+}$, $[Ru(bpy)(dab)_2]^{2+}$, and $[Ru(dab)_3]^{2+}$ in comparison with $[Ru(bpy)_3]^{2+}$. MDCT: Metal-to-ligand charge transfer from Ru to the diazabutadiene ligand. MBCT: Metal-to-ligand charge transfer Ru to the bipyridine ligand.

function of stoichiometry (Figure 3), a linear relationship clearly appears with the number of dab ligands. As it is possible to correlate qualitatively first oxidation and reduction potentials with the HOMO and LUMO energies (extended Koopmans' theorem),[36] this behavior is consistent with the concept that electrochemical potentials are additive with respect to ligand substitution. The additivity of electrochemical potentials was verified for a wide range of complexes.[37] In fact, this is a very general observation common to both organometallic and coordination chemistry.

3.2. Excited States. 3.2.1. Excitation Energies. The absorption spectrum has been calculated by TD-DFT method for each complex. Principal interesting transitions (oscillator strengths $f > 0.07$) are reported in Table 2. Simulated absorption spectra of the three complexes are shown in Figure 4, along with the spectrum of $[Ru(bpy)_3]^{2+}$ for comparison.

The lowest strong energy bands in each complex are MLCT transitions from Ru(4d) orbitals to $d\pi^*$ orbitals of dab and bpy ligands. They lie at energies higher than 2.90 eV. Although some mixing occurs, singlet metal-to-bipyridine charge transfer (^{1}MBCT) states and metal to diazabutadiene charge transfer (^{1}MDCT) states can easily be distinguished. In all cases with $x \neq 0$, the lowest transition energy involves ^{1}MDCT excited states, as a consequence of the population of the low-energy π^* orbitals of the dab ligand. Incorporation of two dab ligands results in transitions that lead to a broader absorption band and in a decrease of the oscillator strengths. In Table 3 the lowest vertical ^{1}MLCT transitions to dab or bpy ligands are shown in each complex. For these transitions, our calculations predict very small oscillator strengths ($f < 0.001$). All the other vertical transitions with non-negligible oscillator strengths ($f > 0.01$) are reported in Table S1 in the Supporting Information, but are not discussed here. As expected, ^{1}MDCT states lie at much lower energies than the ^{1}MBCT ones, and one can notice that inclusion of more dab ligands in the coordination sphere pushes the ^{1}MBCT transitions toward higher energies. Moreover, for the $[Ru(bpy)(dab)_2]^{2+}$ complex, the absorption bands corresponding to ^{1}MDCT and ^{1}MBCT transitions are well separated in contrast to the absorption spectrum of $[Ru(bpy)_2(dab)]^{2+}$. Thus, it should be possible to selectively

Table 3. Lowest Vertical MLCT and MC Singlet Transitions (eV) Obtained with TD-DFT

	^{1}MDCT[a] ($f \approx 0$)	^{1}MBCT[b] ($f \approx 0$)	^{1}MC ($f \approx 0$)
complex	$dz^2\rightarrow d\pi^*$	$dz^2\rightarrow d\pi^*$	$dz^2\rightarrow d\sigma^*$
$[Ru(bpy)_3]^{2+}$		2.47	>3.90[c]
$[Ru(bpy)_2(dab)]^{2+}$	1.70	2.92	3.82
$[Ru(bpy)(dab)_2]^{2+}$	1.90	3.39	3.96
$[Ru(dab)_3]^{2+}$	2.04		4.08

[a] MDCT: Metal-to-ligand charge transfer from Ru to the diazabutadiene(s). [b] MBCT: Metal-to-ligand charge transfer from Ru to the bipyridine(s). [c] ^{1}MC state not found in the first 20 singlet states computed.

(36) (a) Perdew, J. P.; Levy, M. *Phys. Rev. B* **1997**, *56*, 16021−16028, and references therein. (b) Chong, D. P.; Gritsenko, O. V.; Baerends, E. J. *J. Chem. Phys.* **2002**, *116*, 1760–1772. (c) Gritsenko, O.; Baerends, E. J. *Can. J. Chem.* **2009**, *87*, 1383–1391.

(37) (a) Dodsworth, E. S.; Lever, A. B. P. *Chem. Phys. Lett.* **1986**, *124*, 152–158. (b) Lever, A. B. P. *Inorg. Chem.* **1990**, *29*, 1271–1285. (c) Duff, C. M.; Heath, G. A. *Inorg. Chem.* **1991**, *30*, 2528–2535.

Table 4. Main Bond Lengths (Å) and Bond Angles (deg) in C_2 Symmetry for the Lowest ^{3}MLCT state of $[Ru(bpy)_2(dab)]^{2+}$, $[Ru(bpy)(dab)_2]^{2+}$, and $[Ru(dab)_3]^{2+}$ and for the Lowest ^{3}MC State of $[Ru(bpy)_2(dab)]^{2+}$ and $[Ru(dab)_3]^{2+}$

	$[Ru(bpy)_2(dab)]^{2+}$	$[Ru(bpy)(dab)_2]^{2+}$	$[Ru(dab)_3]^{2+}$	$[Ru(bpy)_2(dab)]^{2+}$	$[Ru(dab)_3]^{2+}$
	MLCT ^3B	MLCT ^3B	MLCT ^3B	MC $^3A^a$	MC ^3A
$\langle S^2\rangle$	2.008	2.008	2.006	2.083	2.050
			Geometry		
$Ru-N_{dab}$	2.030	2.048, 2.031	2.016, 2.060, 2.096	2.032	2.044, 2.476, 2.123
$Ru-N_{bpy}$	2.097, 2.122	2.116		2.432, 2.171	
$(N-C)_{dab}$	1.351	1.317, 1.319	1.343, 1.291, 1.291	1.308	1.300, 1.274, 1.281
$(N-C)_{bpy}$	1.360, 1.359	1.360		1.346, 1.358	
$(C-C)_{dab}$	1.385	1.419	1.394, 1.455	1.427	1.438, 1.477
$(C-C)_{bpy}$	1.473	1.471		1.482	
$(N-Ru-N)_{dab}$	78.6	77.2	78.4, 75.2	76.0	75.6, 69.9
$(N-Ru-N)_{bpy}$	77.6	77.2		71.7	
			Spin Density		
Ru	0.98	0.92	0.88	1.98	1.95
dab	1.04	2×0.54	0.94, 2×0.09	−0.17	−0.10, 2×0.08
bpy	2×-0.01	0.00		2×0.10	

[a] Saddle point on the PES.

populate the singlet MDCT or MBCT excited state of $[Ru(bpy)(dab)_2]^{2+}$ initially by tuning the wavelength of the irradiation source. Different behavior may be expected from these initially excited singlet states, in particular with the view of ultrafast photoinduced electron transfer applications for example.[1,2,38]

In the case of the homoleptic $[Ru(dab)_3]^{2+}$ complex, one can note that we predict two absorption bands, a weak one around 500 nm (see Table S1 in Supporting Information) and an intense peak around 400 nm (see Figure 4 and Table 2). Qualitatively, this is in good agreement with the absorption bands found at 550 and 425 nm with respective molar extinction coefficients of 8500 and 30500 L mol^{-1} cm^{-1} for a homoleptic substituted diazabutadiene Ru^{II} complex.[32] Note that, not only the positions of the bands, but also the intensities, are well reproduced. However, whereas these transitions were assigned to a ^{1}MLCT state and a $^1(\pi\rightarrow\pi^*)$ state respectively, both peaks correspond to ^{1}MLCT states in $[Ru(dab)_3]^{2+}$.

It is worth noticing that, contrary to our previous studies,[12,13] ^{1}MC states appear within the 20 singlet roots in the calculated absorption spectra for all the cases with $x \neq 0$. The corresponding transition energies range from 3.82 to 4.08 eV (see Table 3). Thus, unlike the ^{1}MLCT states, the transition to the ^{1}MC states is not very sensitive to the substitution of bpy ligands by dab ligands. This means that such a substitution does not notably perturb the dσ bonding scheme of those complexes.

3.2.2. Lowest Triplet MLCT States. The lowest triplet states of each compound were investigated using UB3LYP calculations followed by geometry optimization and harmonic frequency analysis. Starting from the corresponding molecule in its ground state, an MLCT ^3B state was found for all complexes as the lowest triplet state. For each compound and electronic state, the optimized geometric parameters are given in Table 4 along with the value of $\langle S^2\rangle$ (typically 2.006 to 2.008). All the C_2 structures detailed herein are true minima on the triplet PES. The nature of these states can be determined by analysis of the corresponding singly occupied orbitals depicted in Figure 5. In all the cases, the two singly occupied molecular orbitals (SOMOs) of the optimized ^{3}MLCT structures correspond to the HOMO and LUMO obtained in the ground-state geometry (compare Figures 2 and 5). The introduction of a strong π-acceptor ligand has the effect of localizing the excitation (promoted electron) onto the dab ligand(s), giving a ^{3}MDCT as the lowest triplet excited state. These triplet states show great similitude with the one of $[Ru(bpy)_3]^{2+}$ and can be viewed as the distribution of one electron on the ruthenium center while the other is spread over the dab ligand(s). The ruthenium is formally oxidized as Ru^{III} with reduction of the dab ligand(s). All these descriptions are consistent with the following: (i) the contraction of the $Ru-N_{dab}$ bonds in the ^{3}MLCT state with respect to the ground state, because of electrostatic attractive interaction between the trication and the electron spread over the dab ligand(s), (ii) the decrease of the π bonding character in the CN bond and the increase of the π bonding character in the CC bonds with respect to the ground state, resulting from the population of the SOMO. The first bond is thus lengthened and the last one shortened in the ligand accommodating the electronic density in each excited triplet state, and (iii) the values of the Mulliken spin density for each ligand in each complex displayed in the last rows of Table 4.

A noticeable difference is the location of the promoted electron in the $[Ru(dab)_3]^{2+}$ case. Indeed, the promoted electron is mainly localized on a single dab ligand. This point is consistent with the occupation of a SOMO displaying a large electron density on one of the three ligands. The situation is different in $[Ru(bpy)_3]^{2+}$ and also in $[Ru(tap)_3]^{2+}$, for which localization of the promoted electron over two ligands is mainly observed.[39,12,13] Note that in reference 39, solvent and dynamic effects were

(38) She, C.; Guo, J.; Irle, S.; Morokuma, K.; Mohler, D. L.; Zabri, H.; Odobel, F.; Youm, K.-T.; Liu, F.; Hupp, J. T.; Lian, T. *J. Phys. Chem. A* **2007**, *111*, 6832–6842.

(39) Moret, M.-E.; Tavernelli, I.; Chergui, M.; Rothlisberger, U. *Chem.—Eur. J.* **2010**, *16*, 5889–5894.

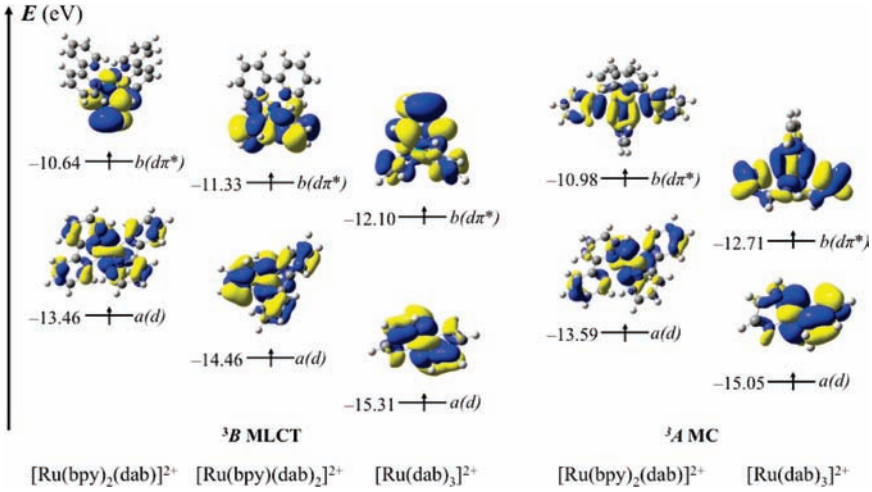

Figure 5. Simplified molecular orbital diagram of the SOMOs in C_2 symmetry for the lowest ^{3}MLCT and ^{3}MC states. Orbital eigenvalues are given in eV.

Table 5. Relative Energies (in eV) between the Triplet Excited States and Energy Differences (in eV) between Triplet and Ground States for the $[Ru(bpy)_{3-x}(dab)_x]^{2+}$ ($x = 0-3$) Series Calculated by the DFT Method

complex	$\Delta E_{MLCT\rightarrow MC}$[a]	$\Delta E_{MLCT\rightarrow GS}$[b]	$\Delta E_{MC\rightarrow GS}$[c]
$[Ru(bpy)_3]^{2+}$	−0.08	2.10	1.08
$[Ru(bpy)_2(dab)]^{2+}$	0.96	0.84	1.09
$[Ru(bpy)(dab)_2]^{2+}$		1.05	
$[Ru(dab)_3]^{2+}$	0.57	1.21	0.88

[a] Relative energies of the ^{3}MC state relative to ^{3}MLCT at their respective B3LYP geometries. [b] Vertical transition energies of the ^{3}MLCT state at the B3LYP geometries. [c] Vertical transition energies of the ^{3}MC state at the B3LYP geometries.

taken into account, while our argument is based on electron density found in the gas phase.

In the second column of Table 5, the electronic energy differences between the triplet MLCT state and the ground state of each complex are given. These transition energies were computed by Δ-SCF calculations at the optimized ^{3}MLCT state geometry, which provide a good estimate of the emission energies. The emission energies are 0.84, 1.05, and 1.21 eV for the $[Ru(bpy)_2(dab)]^{2+}$, $[Ru(bpy)(dab)_2]^{2+}$, and $[Ru(dab)_3]^{2+}$ complexes, respectively. These results mean that the emission energies of the lowest MLCT ^3B state occur in the infrared region (in the range of ca. 1000−1500 nm). In previous papers calculated emission energies of the MLCT ^3B were reported in the visible spectrum at 590 nm, 568, and 544 nm for the $[Ru(bpy)_3]^{2+}$, $[Ru(bpz)_3]^{2+}$, and $[Ru(tap)_3]^{2+}$ complexes, respectively.[12,13] The shift of the emission energies toward the infrared region is a result of the large stabilization of the ^{3}MLCT states because of the strong π-acceptor dab ligands.

3.2.3. Triplet MC States. Starting from the optimized ^{3}MLCT, judicious $Ru-N_{bpy}$ or $Ru-N_{dab}$ bond distances were elongated to obtain initial guess geometries. Each optimized structure was confirmed to be either a minimum or a saddle point by performing harmonic frequency calculations. As shown by the spin density values and by principal geometrical parameters given in Table 4, the obtained triplet states are all ^{3}MC states of C_2 symmetry. The SOMOs are schematized in Figure 5. In $[Ru(bpy)_2(dab)]^{2+}$, the excited electron is promoted in the antibonding σ^* orbital mainly localized along the N−Ru−N bond of the two trans bpy ligands, whereas in $[Ru(bpy)(dab)_2]^{2+}$ the electron density associated with the excited electron is mainly localized on the antibonding σ^* orbital along the N−Ru−N bond of the two trans dab ligands. As a result, one can observe an elongation of the two $Ru-N_{bpy}$ and $Ru-N_{dab}$ bond lengths up to about 2.45 Å.

The most striking difference concerns the nature of the optimized structures. A minimum was located on the triplet PES for the $[Ru(dab)_3]^{2+}$, whereas only a saddle-point was found for the $[Ru(bpy)_2(dab)]^{2+}$ complex and no ^{3}MC stationary point could be determined for the $[Ru(bpy)(dab)_2]^{2+}$ complex.[40] The topology of the triplet PES will be further discussed in the next subsection.

The transition energies computed by Δ-SCF at the MC ^3A state optimized geometry are 1.09 and 0.88 eV for the $[Ru(bpy)_2(dab)]^{2+}$ and $[Ru(dab)_3]^{2+}$ complexes, respectively. The region of this spectrum is seldom scrutinized, but as we have shown in a recent study,[41] the ^{3}MC state is not an emissive state for the $[Ru(bpy)_3]^{2+}$ complex. Note that similar transition energies were obtained for the $[Ru(bpy)_3]^{2+}$, $[Ru(bpz)_3]^{2+}$, and $[Ru(tap)_3]^{2+}$ complexes,[12,13] which show that the dab ligands do not notably perturb the dσ bonding scheme of the complexes leaving the ^{3}MC state unaffected by the ligand substitution.

3.3. Topology of the Triplet PES along the MLCT→MC Relaxation Pathway. The relative energies of the ^{3}MLCT and ^{3}MC states have been scrutinized to assess the potential efficiency of the luminescence of the studied complexes. The first column in Table 5 gives these relative energies for each complex of the $[Ru(bpy)_{3-x}(dab)_x]^{2+}$ ($x = 0-3$) series. In contrast to $[Ru(bpy)_3]^{2+}$ for which the triplet MC state is lower than the triplet MLCT state, all the complexes with dab ligands have an MLCT ^3B state as their lowest relaxed triplet state. As mentioned before, the dab ligands do not notably perturb the dσ bonding scheme of the complexes; thus the triplet MC state is not much affected in terms of energy. Therefore, the large stabilization of the ^{3}MLCT relative to the ^{3}MC states mainly results

(40) All our attempts at finding a ^{3}MC stationary points failed for the $[Ru(bpy)(dab)_2]^{2+}$ complex. We could only find a structure corresponding to a small energy gradient (flat region on the triplet PES) but the gradient never vanished.

(41) Heully, J.-L.; Alary, F.; Boggio-Pasqua, M. *J. Chem. Phys.* **2009**, *131*, 184308.

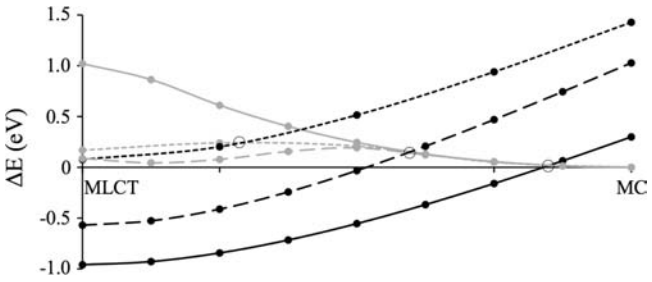

Figure 6. Potential energy profiles along an approximate ^{3}MLCT→^{3}MC reaction path: UB3LYP linear interpolation between MLCT ^3B and MC ^3A states. Black and gray curves correspond to ^3B and ^3A energies, respectively. Results for $[Ru(bpy)_2(dab)]^{2+}$ in full line, results for $[Ru(dab)_3]^{2+}$ in long dashed line, results for $[Ru(bpy)_3]^{2+}$ in short dashed line. Open circles indicate the state crossings.

from the lowering of the ^{3}MLCT state because of the strong π-acceptor dab ligands, and for all the complexes with dab ligands the ^{3}MC state lies at a much higher energy than the ^{3}MLCT state.

Figure 6 presents the potential energy profiles along an approximate ^{3}MLCT→^{3}MC reaction path for the $[Ru(bpy)_3]^{2+}$, the $[Ru(bpy)_2(dab)]^{2+}$, and the $[Ru(dab)_3]^{2+}$ complexes. These profiles were obtained by computing the energies of the ^3B and ^3A states at linearly interpolated geometries between the MLCT ^3B and the MC ^3A C_2 structures. As shown in Figure 6 and explained in a previous article,[13] the ^3B and ^3A states cross along this reaction path (see open circles in Figure 6). The crossing point corresponds to a conical intersection between the two states and, if we consider the second degeneracy-lifting coordinate (corresponding to the non-adiabatic coupling vector), two minimum energy paths appear on the lowest adiabatic triplet energy surface. These minimum energy paths involve transition states lying on each side of the conical intersection as illustrated in Figure 7a. This is what happens in the case of the $[Ru(bpy)_3]^{2+}$ complex, for which the MC ^3A state is a true minimum. However, the situation is different for the $[Ru(bpy)_2(dab)]^{2+}$ complex, as the MC ^3A state is a first order saddle point, which does not connect two distinct minima. This saddle point is in fact a bifurcating point leading back to the MLCT ^3B global minimum via two symmetrically equivalent relaxation pathways on each side of the conical intersection (see Figure 7b). This has been verified by performing intrinsic reaction coordinate (IRC) calculations and energy minimizations following both directions of the transition vector characterizing the MC ^3A state. It is likely that this topology is due to the electronic coupling between the two states, as the MC ^3A structure lies very close to the conical intersection as shown in Figure 6. For the $[Ru(dab)_3]^{2+}$ complex, the MC ^3A structure corresponds to a true minimum, and the triplet surface topology is similar to that of the $[Ru(bpy)_3]^{2+}$ complex apart from the fact that the MC ^3A minimum lies at a much higher energy than the MLCT ^3B minimum. Note that we could not locate any stationary point on the MC ^3A state of the $[Ru(bpy)(dab)_2]^{2+}$ complex. We only found a flat region of the triplet surface corresponding to the MC ^3A state, but the energy gradient never vanished. A possible explanation is that the MC ^3A minimum does not lie on the lowest adiabatic triplet PES but on the second or higher triplet PES because of a change in the $^3B/^3A$ conical intersection topology (from "peaked" to "sloped"). Alternatively, it is possible that no stationary point exists for the MC ^3A state of this complex, that is, no stable structure is associated with the ^{3}MC state of the $[Ru(bpy)(dab)_2]^{2+}$ complex.

As a result of the high energy of the triplet MC state relative to the triplet MLCT state in the complexes $[Ru(bpy)_{3-x}(dab)_x]^{2+}$ (with $x = 1-3$), we theoretically predict that the excited-state lifetime of the triplet MLCT state will be much higher than in the $[Ru(bpy)_3]^{2+}$ complex. Because the triplet MC state either does not correspond to a stable structure ($[Ru(bpy)_2(dab)]^{2+}$ and $[Ru(bpy)(dab)_2]^{2+}$) or is simply too high in energy ($[Ru(dab)_3]^{2+}$), this state will not be populated and cannot quench the photoluminescence of the triplet MLCT state. Thus, we expect higher emission quantum yield for the series $[Ru(bpy)_{3-x}(dab)_x]^{2+}$ (with $x = 1-3$). However, because of the large stabilization of the triplet MLCT state when at least one dab ligand is present, the photoluminescence of these complexes will take place in the near-infrared region (in the range 1000−1500 nm) as shown by the transition energies in Table 5 ranging from 0.84 to 1.21 eV. These complexes, although not interesting for visible light-emitting diodes, could be potential candidates for near-infrared light-emitting diodes or near-infrared emitting probes.[42] Moreover, we have shown that the energy level of the singlet and triplet MLCT states can be tuned by the use of the dab ligand. This ligand can therefore be useful to adjust the energy of the excited state populated after photoabsorption of ruthenium(II) complexes opening new perspectives for photoinduced electron transfer applications.[2,9,43]

3.4. Ab Initio Benchmark Calculations. To assess the reliability of the DFT approach in computing structural and energy features of ground and excited states of ruthenium complexes, we have performed some high-level ab initio calculations on the $[Ru(dab)_3]^{2+}$ complex. The fairly small size of this complex allows one to test a wide range of highly correlated ab initio methods and compare these results against the DFT ones. Before discussing these results, it should be recalled that the convergence of the energies with the size of the basis set differs between DFT and highly correlated ab initio methods. The triple-ζ plus polarization basis set that we used probably ensures that the DFT relative energies are converged, but this is certainly not the case for the ab initio calculations, as these energies would still vary upon increasing the size of the basis set. Unfortunately, highly correlated ab initio calculations with much larger basis sets would be prohibitively expensive. Thus, comparison between DFT and ab initio methods using our triple-ζ plus polarization basis set should be taken with care.

(42) (a) Treadway, J. A.; Strouse, G. F.; Ruminski, R. R.; Meyer, T. J. *Inorg. Chem.* **2001**, *40*, 4508–4509. (b) Bergman, S. D.; Gut, D.; Kol, M.; Sabatini, C.; Barbieri, A.; Barigelletti, F. *Inorg. Chem.* **2005**, *44*, 7943–7950. (c) Adams, C. J.; Fey, N.; Weinstein, J. A. *Inorg. Chem.* **2006**, *45*, 6105–6107. (d) Nonat, A. M.; Quinn, S. J.; Gunnlaugsson, T. *Inorg. Chem.* **2009**, *48*, 4646–4648. (e) Chen, J.-L.; Chi, Y.; Chen, K.; Cheng, Y.-M.; Chung, M.-W.; Yu, Y.-C.; Lee, G.-H.; Chou, P.-T.; Shu, C.-F. *Inorg. Chem.* **2010**, *49*, 823–832.

(43) (a) Kirsch-De Mesmaeker, A.; Lecomte, J.-P.; Kelly, J. M. *Top. Curr. Chem.* **1996**, *177*, 25–76. (b) Bijeire, L.; Elias, B.; Souchard, J.-P.; Gicquel, E.; Moucheron, C.; Kirsch-De Mesmaeker, A.; Vicendo, P. *Biochemistry* **2006**, *45*, 6160–6169. (c) Boggio-Pasqua, M.; Vicendo, P.; Oubal, M.; Alary, F.; Heully, J.-L. *Chem.—Eur. J.* **2009**, *15*, 2759–2762.

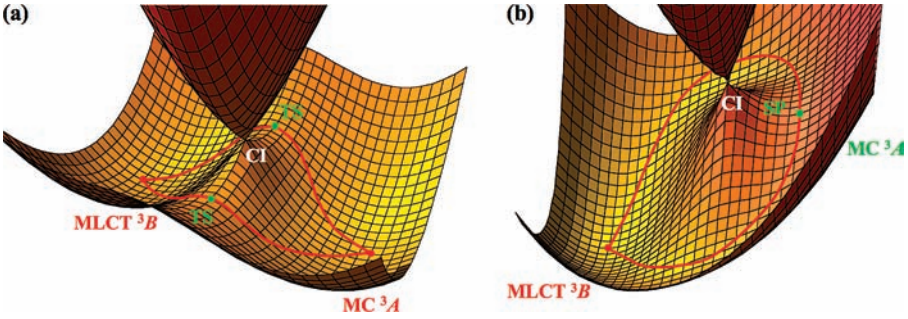

Figure 7. Topology of the triplet PES: comparison between (a) the $[Ru(bpy)_3]^{2+}$ complex, and (b) the $[Ru(bpy)_2(dab)]^{2+}$ complex. The red curves represent the minimum energy pathways between the MLCT ^3B and MC ^3A structures. CI: conical intersection, TS: transition state, SP: saddle point.

Table 6. Main Bond Lengths (Å) and Angles (deg) for the Ground-State D_3 Structure of the $[Ru(dab)_3]^{2+}$ Complex Optimized with Various High-Level Ab Initio Methods

methods	$Ru-N_{dab}$	$(N-C)_{dab}$	$(C-C)_{dab}$	$(N-Ru-N)_{dab}$	$(N-Ru-N)_{trans}$
B3LYP	2.064	1.291	1.454	75.3	166.8
CASSCF[a]	2.134	1.257	1.485	74.4	168.4
MP2	1.967	1.318	1.431	76.6	164.9
MP3	2.085	1.280	1.478	75.8	169.6
MP4(SDQ)[b]	2.034	1.293	1.467	76.1	168.3
QCISD	2.056	1.292	1.468	76.0	168.5
CCSD	2.065	1.287	1.472	75.8	168.9

[a] Using a (10e,10o) active space. [b] No triple substitutions were included because of lack of analytic energy gradients available for full MP4.

Ground-state geometry optimizations were performed with CASSCF, MP2, MP3, MP4(SDQ), QCISD, and CCSD ab initio levels for which analytic energy gradients are available. The main geometrical parameters are collected in Table 6. The B3LYP optimized structure compares very well with the ones obtained at the MP3, MP4(SDQ), QCISD, and CCSD levels. In fact it is in excellent agreement with the geometry obtained at the highest level of theory (CCSD). Only CASSCF and MP2 show a strong deviation with all the other correlated methods. With the CASSCF method, the predicted ground-state geometry is only qualitatively correct. This method suffers from a lack of dynamic electron correlation because of the fairly small configuration interaction performed among the active orbitals (only 10 electrons were distributed among 10 orbitals, see Figure S1 in Supporting Information). Thus, it is not surprising to obtain Ru−N bond distances that are too long. The double bond character of the N−C bond is also too pronounced, while the C−C bond is too long because of a lack of electron delocalization. With the MP2 approach, the predicted ground-state geometry is not even qualitatively correct. In fact, the lowest energy structure displays a trigonal prismatic D_{3h} geometry (Figure S2 in Supporting Information). The pseudo-octahedral D_3 structure lies at a higher energy and does not correspond to a stable structure on the MP2 ground-state PES. This is a result of a bad behavior of the second-order energy correction computed in the perturbation theory. In all the other methods the trigonal prismatic D_{3h} structure corresponds to a high energy point on the ground-state PES. Moreover, the pseudo-octahedral D_3 structure optimized with MP2 displays far too short Ru−N distances. The bond lengths within the dab ligand are also not accurate, with the N−C bond slightly too long and the C−C bond too short.

Triplet excited-state geometry optimizations were also performed using unrestricted MP2 and MP3 to compare with the DFT relaxed structures obtained for the MLCT

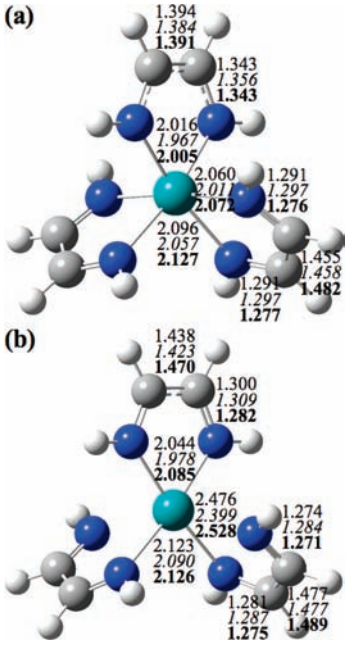

Figure 8. Optimized C_2 structures on the triplet PES of the $[Ru(dab)_3]^{2+}$ complex. (a) MLCT ^3B minimum geometry, and (b) MC ^3A minimum geometry. Bond lengths are in angstroms. UDFT results in normal font, UMP2 results in italics, and UMP3 results in bold font.

^3B and MC ^3A states. Higher-level of theory such as MP4(SDQ), QCISD, and CCSD are computationally too expensive to perform an energy gradient calculation with a reference unrestricted wave function on this system at present. Figure 8 collects the main interatomic distances obtained at the unrestricted DFT, MP2, and MP3 levels. One can see that the DFT geometry is in better agreement with the MP3 level. The geometries of the dab ligands are in good agreement between all three levels of theory. For the Ru−N distances, as observed in the ground-state geometry, MP2 tends to give metal−ligand

Table 7. Relative Energies between the Triplet Excited States (MLCT and MC) and the Ground State (GS) in the $[Ru(dab)_3]^{2+}$ Complex Calculated with Various High-Level Ab Initio Methods

methods	$\Delta E_{MLCT \rightarrow MC}$ [a]	$\Delta E_{MLCT \rightarrow GS}$ [b]	$\Delta E_{MC \rightarrow GS}$ [c]
B3LYP	0.57	1.21	0.88
TD-B3LYP	0.57	1.17	0.84
HF	−0.53	0.45	0.27
MP2	0.49	1.77	0.65
MP3	0.04	1.23	0.59
MP4(SDQ)	0.24	1.58	0.71
MP4(SDTQ)	0.48	1.86	0.78
QCISD	0.26	1.54	0.73
QCISD(T)	0.42	1.49	0.82
CCSD[d]	0.21	1.39	0.71
CCSD(T)	0.39	1.52	0.79
CASSCF	−0.35	0.92	0.55
CASPT2	0.62	1.11	0.28
CIPT2	0.71	1.19	0.42

[a] Relative energies of the ^{3}MC state relative to ^{3}MLCT at their respective B3LYP geometries. [b] Vertical transition energies of the ^{3}MLCT state at its B3LYP geometry. [c] Vertical transition energies of the ^{3}MC state at its B3LYP geometry. [d] T1 diagnostic: 0.032 for ^{3}MLCT, 0.028 for ^{3}MC. All energies are in eV. The blank lines separate the DFT approaches, from the monoreference ab initio methods based on an Hartree−Fock (HF) wave function and the multireference ab initio methods based on a CASSCF wave function.

distances that are too short, while these distances are slightly too long with MP3. The fact that, the DFT Ru−N bond distances are enclosed by the MP2 and MP3 values, gives us confidence that DFT gives accurate metal−ligand distances. Indeed, for the ground-state structure, the more accurate MP4(SDQ), QCISD, and CCSD methods also gave Ru−N bond lengths that were surrounded by the MP2 and MP3 values (see Table 6).

In Table 7 we report the energy differences between triplet excited states and the ground state of $[Ru(dab)_3]^{2+}$ calculated with highly correlated ab initio methods. First, we focus on the relative energy between the ^{3}MLCT and ^{3}MC states, which is a very important parameter for the photophysical properties of ruthenium polypyridine complexes as it largely controls the excited-state lifetime and fluorescence efficiency of the ^{3}MLCT state.[41] The B3LYP value for this relative energy is computed at 0.57 eV with the ^{3}MLCT state being the lowest relaxed triplet excited state. Two methods predict the ^{3}MC state as the lowest excited state. These are the Hartree−Fock (HF) and the complete active space self-consistent field (CASSCF) methods. Both of them suffer from a serious lack of electron correlation, and the poor energetics obtained with these methods are not surprising. Correlated methods using the HF wave function as a reference (monoreference methods) all predict the ^{3}MLCT state lower in energy than the ^{3}MC state. With the highest levels of calculation using perturbation theory (full MP4, denoted MP4(SDTQ)), configuration interaction approaches (QCISD(T)), and coupled-cluster theory (CCSD(T)) we found an energy difference between 0.4 and 0.5 eV. Multireference methods using the CASSCF wave function as a reference predict a higher relative energy of 0.62 and 0.71 eV with CASPT2 and CIPT2, respectively. Overall, the DFT value looks reliable as it is encompassed between the best monoreference and multireference methods.

Second, we are looking at the energy difference between the ^{3}MLCT and ground states calculated at the ^{3}MLCT optimized structure. This transition energy gives a good estimate of the emission energy of the complexes. This energy difference is computed at 1.21 eV with B3LYP. Again, HF and CASSCF values are fairly poor with far too low transition energies. Monoreference methods systematically predict a higher emission energy than the B3LYP value. On the other hand, the agreement is very good with the multireference methods with deviations of only 0.10 and 0.02 eV with the CASPT2 and CIPT2 values, respectively. The CASPT2 method is probably among the most used ab initio method to compute transition energies and is acknowledged to compute these transitions with errors of less than 0.3 eV for low-lying excited states.[44] CIPT2 is probably even more accurate as it relies on the same perturbation theory but using a better reference wave function than CASPT2. Therefore, we are confident that DFT can compute reliable emission energies for ^{3}MLCT states. In support of this statement, a good agreement with experimental emission energies has already been obtained for some ruthenium polypyridine complexes.[12,13]

Finally, we compare the energy difference between the ^{3}MC and ground states calculated at the ^{3}MC optimized structure. This energy difference is not as important as the two previous ones described above because it is not an experimental observable. Indeed, the ^{3}MC state is not emissive; however, the system can decay back to the ground state from this triplet state via a surface crossing.[41] Thus, this energy difference gives an indication of the proximity of the crossing with the ^{3}MC minimum. It is computed at 0.88 eV with B3LYP. The best monoreference methods predict a transition energy of about 0.8 eV, whereas 0.4 eV is obtained with the best multireference method. Assuming CIPT2 is the most accurate of all methods, the DFT value seems too large. However, it is important to note that this energy difference is very sensitive to the geometry. The reason is that the ^{3}MC state has a shallow minimum with a very flat PES along the decoordinated Ru−N bond distances, whereas along these coordinates, the ground-state PES is highly attractive (the ground-state energy rises very steeply as the Ru−N bond lengths increase bringing the ground state and ^{3}MC state close in energy). Thus, a substantial change in the decoordinated Ru−N distances (i.e., from 2.45 to 2.50 Å) would not change the ^{3}MC state energy very much but the ground state energy would. As all the ab initio computations in Table 7 have been performed at the B3LYP optimized structures, it is likely that the ab initio transition energy of the ^{3}MC state would change significantly if one could reoptimize the ^{3}MC minimum with the ab initio method itself. For example, the MP3 value is 0.59 eV using the DFT geometry, but is 0.43 eV when using the optimized MP3 geometry of Figure 8.

One can also note the very good agreement between the DFT and TD-DFT results. In particular, the fact that the emission energies from the ^{3}MLCT state ($\Delta E_{MLCT \rightarrow GS}$) are very close shows that TD-DFT is reliable in this case to compute transition energies of charge transfer states. This is due to the short-range charge transfer nature of these excited states. In addition, we also performed CASPT2 calculations using a correlation-consistent polarized valence

(44) Pierloot, K. *Mol. Phys.* **2003**, *101*, 2083–2094.

quadruple-ζ basis set (cc-pVQZ)[45] on the hydrogen, carbon, and nitrogen atoms, and used two f and one g basis functions on the ruthenium center[22] to assess the basis set convergence with this approach. We obtained an emission energy from the ^{3}MLCT state of 1.11 eV, identical to the one obtained with the smaller basis set. The ^{3}MC state lies 0.95 eV above the ^{3}MLCT state, that is, 0.33 eV higher up in energy. $\Delta E_{MC \rightarrow GS}$ was computed at 0.24 eV, very close to the smaller basis set result. The fact that the computed emission energy is stable and that the ^{3}MC state remains largely above the ^{3}MLCT state confirms the overall photophysical model obtained with our DFT approach.

4. Conclusion

We have carried out a comparative study of the Ru(II) complexes $[Ru(bpy)_{3-x}(dab)_x]^{2+}$ ($x = 1-3$) and compared their predicted photophysical properties to the ones of the reference complex $[Ru(bpy)_3]^{2+}$. We have shown that the presence of a dab ligand changes dramatically these properties because of the strong π-acceptor character of this ligand. The main effect is a substantial energy lowering of the MLCT states leading to several important consequences: (i) a strong red-shift of the maximum of the ^{1}MLCT absorption band corresponding to MDCT transitions, (ii) a strong decrease of the emission energy of the ^{3}MLCT states compared to the reference complex, with all the $[Ru(bpy)_{3-x}(dab)_x]^{2+}$ ($x = 1-3$) complexes luminescent in the near-infrared region, while $[Ru(bpy)_3]^{2+}$ emits in the visible region, and (iii) the ^{3}MC states become inaccessible in all the $[Ru(bpy)_{3-x}(dab)_x]^{2+}$ ($x = 1-3$) complexes, either because they are too high in energy relative to the ^{3}MLCT states ($[Ru(dab)_3]^{2+}$) or because the ^{3}MC states are unstable ($[Ru(bpy)_2(dab)]^{2+}$ and $[Ru(bpy)(dab)_2]^{2+}$). The consequence could be an improved emission efficiency desirable for applications like diodes and probes.

We have also performed accurate ab initio calculations on the $[Ru(dab)_3]^{2+}$ complex against which to benchmark the DFT results. The B3LYP functional used in this study gave very good results in terms of ground- and excited-state structures. As far as the energetics are concerned, it provided reliable results for the relative energy between the ^{3}MLCT and ^{3}MC states and for ^{3}MLCT emission energies.

Acknowledgment. We thank CALMIP (www.calmip.cict.fr) for access to computing resources.

Supporting Information Available: List of Cartesian coordinates for optimized DFT and ab initio structures. Table S1 for complete absorption spectrum obtained with TD-DFT. Figure S1 for the active space chosen in the CASSCF approach. Figure S2 for the trigonal prismatic D_{3h} geometry obtained at the MP2 level. This material is available free of charge via the Internet at http://pubs.acs.org.

(45) Dunning, T. H., Jr. *J. Chem. Phys.* **1989**, *90*, 1007–1023.